TIME DOMAIN FULL WAVEFORM INVERSION OF SEISMIC DATA FOR THE EAST SEA, KOREA, USING A PSEUDO-HESSIAN METHOD WITH SOURCE ESTIMATION

JIHO HA[1], SUNGRYUL SHIN[2], CHANGSOO SHIN[3] and WOOKEEN CHUNG[4]

[1] *Department of Energy and Resources Engineering, Korea Maritime and Ocean University, Busan, South Korea.*
[2] *Department of Energy and Resources Engineering, Korea Maritime and Ocean University, Busan, South Korea.*
[3] *Department of Energy Systems Engineering, Seoul National University, Seoul, South Korea.*
[4] *Department of Energy and Resources Engineering, Korea Maritime and Ocean University, Busan, South Korea. wkchung@kmou.ac.kr*

(Received July 25, 2014; revised version accepted August 4, 2015)

ABSTRACT

Ha, J., Shin, S., Shin, C.S. and Chung, W., 2015. Time domain full waveform inversion of seismic data for the East Sea, Korea, using a pseudo-Hessian method with source estimation. *Journal of Seismic Exploration*, 24: 419-437.

Waveform inversion is used to estimate subsurface velocity information using seismic datasets. To overcome the computational burden, the use of back-propagation algorithm and the pseudo-Hessian matrix are proposed. Many researchers using these algorithms have shown successful results with synthetic and field data tests. In particular, the computational efficiency of waveform inversion is improved by using a pseudo-Hessian with regularization using a virtual source vector. However, these theoretical concepts have been mainly applied to waveform inversion in the frequency or Laplace domains.

We propose full waveform inversion using an estimated source wavelet with the pseudo-Hessian matrix and back-propagation in the time domain. We derive the virtual source vector for the first order hyperbolic equation based on 2D staggered-grid modeling. The updated gradient direction is obtained from both the virtual source and back-propagation wavefield vectors. To improve the availability for field data sets, we also perform the source estimation using deconvolution of the observed data based on the least-squares method.

0963-0651/15/$5.00

In a synthetic test with a modified Marmousi2 model, the inverted velocity model obtained by the proposed waveform inversion algorithm using estimated wavelets shows similarity to the true velocity. The estimated source wavelet shows good agreement with the true source wavelet. We also test the proposed waveform inversion with field data from the East Sea, Korea. The calculated traces with the estimated source wavelet and the inverted velocity model show direct and reflection events similar to those in the real seismic traces. This confirms that the proposed algorithm can be applied to field data.

KEY WORDS: waveform inversion, pseudo-Hessian matrix, back-propagation algorithm, time domain, source estimation, seismic data.

INTRODUCTION

Extracting accurate velocity models from seismic data requires estimating physical properties and seismic imaging. A number of different approaches have been developed to obtain an accurate subsurface velocity model, including travel-time tomography from first arrival information and reflections from seismic traces, estimation of interval properties using well logs or core samples, and seismic waveform inversion. Seismic waveform inversion techniques have been considered an essential step towards a detailed estimation of subsurface properties (Toxopeus et al., 2008; Fichtner, 2011). Since Lailly (1983) and Tarantola (1984) pioneered waveform inversion, many inversion algorithms have been presented in several domains including the time domain (Guthier et al., 1986; Sheen et al., 2006; Choi and Alkhalifah, 2011), the frequency domain (Geller and Hara, 1993; Pratt et al., 1998; Pratt, 1999; Pratt and Shipp, 1999; Shin et al., 2001, Ha et al., 2006; Shin and Min, 2006; Ha et al., 2009) and the Laplace domain (Shin and Cha, 2008; Bae et al., 2010; Koo et al., 2011; Bae et al., 2012). To improve efficiency of full waveform inversion, various forward and inverse problem solutions are developed and applied (Virieux and Operto, 2009). In particular, to acquire more quantitative results of inversion, many approaches for accurate initial velocity model sampling (Koren et al., 1991; Jin and Madariaga, 1993, 1994; Mosegaard and Tarantola, 1995; Sambridge and Mosegaard, 2002) have been proposed (Virieux and Operto, 2009).

Recently, several impedance inversion methods based on linearized approximation for reflectivity is widely utilized (Hampson et al., 2005; Zong et al., 2013). These method have many advantages, however they are limited in complex subsurface structures, especially at high property contrasts between layers or unconformities (Zong et al., 2013). Thus, full waveform inversion based on the complete solution of the two-way wave equation is required to analyze the wave propagation in realistic subsurface structures (Brossier et al., 2009; Fichtner, 2011; Métivier et al., 2014). Full waveform inversion updates the subsurface model parameters iteratively using gradients to minimize the objective function. As a result, waveform inversion needs substantial computational resources. To reduce the computational burden, many waveform

inversion techniques employ the back-propagation algorithm or the pseudo-Hessian matrix (Pratt, 1999; Shin et al., 2001; Shin and Min, 2006; Ha et al., 2009). Both the back-propagation algorithm and the pseudo-Hessian matrix enable efficient calculations and regularize the update direction without explicitly computing the partial derivative wavefield. Most research that employs these methods has used mainly been in the frequency and Laplace domains (Shin et al., 2001; Shin and Min, 2006; Shin and Cha, 2008; Ha et al., 2009). Combination of both methods is not yet used in time domain full waveform inversion.

Below, we apply the pseudo-Hessian method, and the back-propagation technique with virtual sources, to a full waveform inversion in the time domain to calculate and regularize the gradient direction efficiently. The gradient direction is built from both the back-propagated wavefield vector and the virtual source vector. The gradient direction is regularized by the diagonal elements of the pseudo-Hessian matrix. Our modeling algorithm is 2D staggered-grid modeling (Levander,1988; Virieux, 1986). Since the source information is unknown in a field data test, source estimation is an important part of obtaining an accurate velocity model by waveform inversion. Kim et al., (2011) have proposed source estimation for reverse time migration using time-domain least-squares deconvolution. Since source estimation in the frequency domain is required to construct Green's functions to use the full Newton optimization procedure, and to convolve the estimated source wavelet, this method is more expensive than estimation in the time domain (Kim et al., 2011). We also employ source estimation in our waveform inversion. The estimated source is updated at each iteration, and is directly applied in our inversion of field seismic data from the East Sea, Korea.

We focus on the pseudo-Hessian method, the back-propagation technique, and the source estimation in the time domain waveform inversion. First, virtual source vectors for the 2D staggered-grid modeling are derived. We then test the waveform inversion algorithm using numerical data before applying it to field seismic data. The numerical synthetic data used a modified Marmousi2 model in which the water layer was extended to 0.5 km. Then, we perform the waveform inversion of the field data in the time domain.

THEORY

Back-propagation and the pseudo-Hessian matrix in the time domain

For waveform inversion in the time domain, the least squares objective function is

$$E(\mathbf{p}) = \frac{1}{2} \sum_{i=1}^{nsrc} \sum_{j=1}^{nrec} \int_{0}^{T_{max}} [u_{ij}(t) - d_{ij}(t)]^2 dt \quad , \tag{1}$$

where $E(\mathbf{p})$ is the objective function for model parameter ($\mathbf{p}$), nsrc and nrec are the number of sources and receivers, T_{max} and t are the total record time and the time index, and u(t) and d(t) are the calculated and observed data, respectively. From the gradient of the calculated data with respect to each model parameter, we compute the gradient direction of the objective function as:

$$\partial E(\mathbf{p})/\partial p_k = \sum_{i=1}^{nsrc} \int_{0}^{T_{max}} [\partial \mathbf{u}_i(t)^T/\partial p_k] \mathbf{r}_i(t) dt \quad ,$$

$$\mathbf{u}_i(t) = [u_{i1}(t), u_{i2}(t), \cdots, u_{iN}(t)] \quad , \tag{2}$$

$$\mathbf{r}_i(t) = [u_{i1}(t) - d_{i1}(t), u_{i2}(t) - d_{i2}(t), \cdots, u_{inrec}(t) - d_{inrec}(t), 0, \cdots, 0] \quad ,$$

where $\partial \mathbf{u}(t)/\partial p_k$ is the partial derivative wavefield, $\mathbf{u}_i$ and $\mathbf{r}_i$ are the calculated and residual wavefield vectors for the i-th shot, and N is the number of model parameters. The direct calculation of the partial derivative wavefield involves significant computational complexity. The partial derivative wavefield can be defined by the convolution between the Green's function and the virtual source vector as (Chung et al., 2012):

$$\partial \mathbf{u}(t)/\partial p_k = G(t) * \mathbf{v}_{ik}(t) \quad , \tag{3}$$

where G(t) is Green's function, $*$ is the convolution operator and $\mathbf{v}_{ik}(t) = (vs_x, vs_z)$ represents the virtual source vector at the k-th model parameter of the i-th shot to the horizontal (vs_x) and the vertical (vs_z) direction in 2D. The virtual vector is used to compute the partial derivative wavefield with respect to model parameter. It is identical to the forward modeled wavefield (Tarantola, 1984). We define the back-propagated wavefield vector $\mathbf{b}_i(t)$ for the i-th shot for the waveform inversion as:

$$\mathbf{b}_i(t) = G(t) * \mathbf{r}_i(T_{max} - t) \quad . \tag{4}$$

When the partial derivative wavefield in eq. (2) is substituted into eq. (3), the gradient can be reformulated mathematically using eq. (4) as follows:

$$\partial E(\mathbf{p})/\partial p_k = \sum_{i=1}^{nsrc} \int_{0}^{T_{max}} [\partial \mathbf{u}_i(t)^T/\partial p_k] \mathbf{r}_i(t) dt$$

$$= \sum_{i=1}^{nsrc} [\partial \mathbf{u}_i(t)^T / \partial p_k] \otimes \mathbf{r}_i(t)$$

$$= \sum_{i=1}^{nsrc} [G(t) * \mathbf{v}_{i,k}(t)] \otimes \mathbf{r}_i(t)$$

$$= \sum_{i=1}^{nsrc} \mathbf{v}_{i,k}(t) * [G(t) * \mathbf{r}_i(T_{max} - t)]$$

$$= \sum_{i=1}^{nsrc} \mathbf{v}_{i,k}(t) * \mathbf{b}_i(t)$$

$$= \sum_{i=1}^{nsrc} \mathbf{v}_{i,k}(t) \otimes \mathbf{b}_i(T_{max} - t)]$$

$$= \sum_{i=1}^{nsrc} \int_0^{T_{max}} \mathbf{v}_{i,k}(t)^T \mathbf{b}_i(T_{max} - t) dt \quad , \tag{5}$$

where $\otimes$ means zero-lag cross-correlation.

The gradient direction is efficiently calculated using back-propagation without the explicit calculation of the partial derivative wavefield. The gradient direction is scaled by the diagonal elements of the pseudo-Hessian matrix composed of the virtual source vectors (Shin et al., 2001). The diagonal element of pseudo-Hessian matrix in the time domain is:

$$\text{diag}(\mathbf{H}_{pi})_k = \int_0^{T_{max}} \mathbf{v}_{i,k}(t)^T \mathbf{v}_{i,k}(t) dt \quad , \tag{6}$$

where $\mathbf{H}_{pi,k}$ means the k-th pseudo-Hessian matrix for the i-th shot.

The updating of the k-th model parameter at each iteration is expressed as:

$$p_k^{l+1} = p_k^l - s[\sum_{i=1}^{nsrc} \{\text{diag}(\mathbf{H}_{pi})_k + w\}^{-1} \sum_{i=1}^{nsrc} \int_0^{T_{max}} \mathbf{v}_{i,k}^T \mathbf{b}_i(T_{max} - t) dt] \quad , \tag{7}$$

where p_k^l is the k-th model parameter at the l-th iteration, and s and w are the step length for the update, and white noise.

Virtual source vectors for 2D staggered-grid modeling

We explicitly solve the wave equation using the staggered-grid finite-difference method (Virieux, 1986; Levander, 1988; Graves, 1996). Virtual source vectors for both the back-propagation algorithm and the pseudo-Hessian matrix are redefined for the staggered-grid method. In the time domain, the relationship between particle velocity and stress in 2D acoustic media can be written based on the relationship in 2D elastic media (Virieux, 1986):

$$\rho(\partial v_x/\partial t) = (\partial \tau_{xx}/\partial x) + f_x \quad , \tag{8}$$

$$\rho(\partial v_z/\partial t) = (\partial \tau_{zz}/\partial z) + f_z \quad , \tag{9}$$

$$\partial \tau_{xx}/\partial t = \lambda[(\partial v_x/\partial x) + (\partial v_z/\partial z)] + I_{xx} \quad , \tag{10}$$

and

$$\partial \tau_{zz}/\partial t = \lambda[(\partial v_z/\partial z) + (\partial v_x/\partial x)] + I_{zz} \quad , \tag{11}$$

where v_x and v_z are particle velocities, τ_{mn} (m,n = x,z) are stresses, f_x and f_z are source terms of body force, and I_{mn} (m,n = x,z) are traction source terms. Because air-gun arrays are commonly used in general marine seismic surveys, we assume that the source is explosive.

For one value for Lamé's modulus, λ, the equation for the partial derivative wavefield can be written as:

$$(\partial/\partial t)(\partial \tau_{xx}/\partial \lambda^*) = \lambda[(\partial/\partial x)(\partial v_x/\partial \lambda^*) + (\partial/\partial z)(\partial v_z/\partial \lambda^*)] + vs_x \quad , \tag{12}$$

and

$$(\partial/\partial t)(\partial \tau_{zz}/\partial \lambda^*) = \lambda[(\partial/\partial z)(\partial v_z/\partial \lambda^*) + (\partial/\partial x)(\partial v_x/\partial \lambda^*)] + vs_z \quad , \tag{13}$$

where virtual sources are $vs_x = (\partial\lambda/\partial\lambda^*)[(\partial v_x/\partial x) + (\partial v_z/\partial z)]$ and $vs_z = (\partial\lambda/\partial\lambda^*)[(\partial v_z/\partial z) + (\partial v_x/\partial x)]$ to $(\partial/\partial t)(\partial \tau_{xx}/\partial \lambda^*)$ and $(\partial/\partial t)(\partial \tau_{zz}/\partial \lambda^*)$, respectively, λ^* is a virtual source vector parameter for λ for partial derivative wavefield propagation. The virtual source terms are required to calculate the partial derivative wavefield for each property parameter. We solved eqs. (8)-(11) to construct the virtual source terms to eqs. (12) and (13) that show the partial derivative wavefield and the virtual source term for Lame's modulus, λ. Since some of the velocity (v_x and v_z) and stress (τ_{xz}) components don't have a differential factor relative to λ; these become zero. In this study, because the field data are acquired in the East Sea, Korea, we assumed that the data are from an acoustic earth.

To demonstrate our virtual source terms, we generated the virtual source to a perturbation point in the subsurface model shown in Fig. 1. We generated the partial derivative wavefield using the virtual source term [equation (3)] and calculated the partial derivative wavefield using the finite difference method. Fig. 2 shows good agreement between these two approaches.

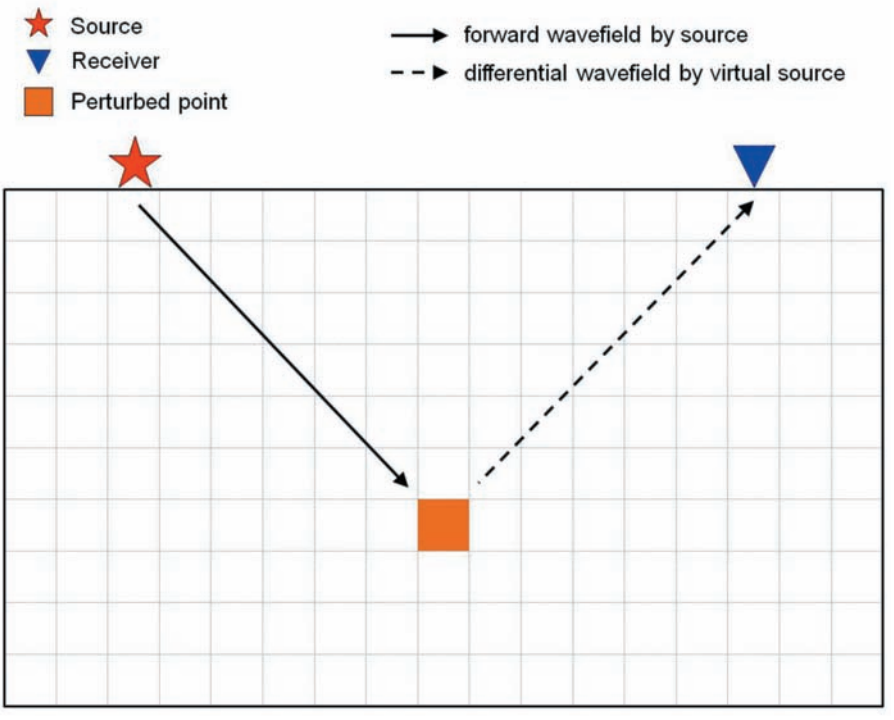

Fig. 1. Schematic diagram of forward and differential wavefield propagation.

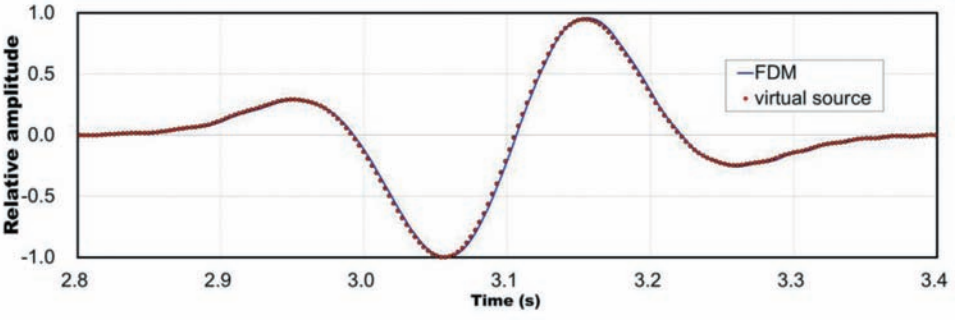

Fig. 2. Comparison of the vertical component partial derivative seismogram for a point perturbation of lambda.

Source estimation in the time domain

The real source signal is not known exactly, but the estimated source should be as similar as possible to the wavelet shape and amplitude of the real field data to perform velocity inversion (Pratt, 1999). When applying the source

estimation to waveform inversion, the difference between the observed and calculated data decreases (Koo et al., 2011). We estimate the source wavelet using the deconvolution method proposed by Kim et al. (2011). The observed data can be described as the convolution result between the Green's function and the source wavelet used:

$$d(t) = \int_0^{T_{max}} G(t) * S(t)\, dt \quad , \tag{14}$$

where S(t) is the source wavelet. The source wavelet can be deconvolved from the observed data based on least-squares fitting (Kim et al., 2011) for which the least-squares error is

$$L = \int_0^{T_{max}} (d(t) - \int_0^{T_{max}} [G_c(t) * S_e(t)]dt)^2 dt \quad , \tag{15}$$

where $G_c(t)$ is the Green's function for the calculated seismic data generation and $S_e(t)$ is the estimated source wavelet.

We calculate the source term by minimizing the least-squares error using the partial derivative of least-squared error with respect to the source term. Then, the cross-correlation between the Green's function and the observed data, and the autocorrelation lags of the Green's function, are computed (Kim et al., 2011). Then, we can obtain the estimated source wavelet from the Levinson algorithm using the characteristics of the Toeplitz matrix (Claerbout, 1971; Kim et al., 2011).

Workflow

The proposed waveform inversion procedure for one iteration is as follows:

1. Estimate the source wavelet from the observed data;
2. Construct the calculated data with the initial model and the estimated source wavelet;
3. Generate the back-propagated residual wavefield using the observed and calculated data;
4. Compose the virtual source vector from the partial derivative wavefield;

5. Construct the gradient and pseudo-Hessian matrix;

6. Update the velocity model.

To demonstrate the proposed waveform inversion algorithm, we perform a numerical test with synthetic data before applying it to the field seismic data.

NUMERICAL EXAMPLE

Modified Marmousi2 model data set

We first apply the proposed waveform inversion algorithm to data from a modified Marmousi2 model in which the water layer is 0.5 km thick and the horizontal extent of the model is 11.0 km [Fig. 3(a)]. Because the field data were acquired in a marine environment, we considered only a P-velocity model where the S-velocity and the density are set to 0 km/s and 1 g/cm^3, respectively. We construct the initial velocity model as a smoothed true velocity model using a module of Seismic Unix (smooth2) to test our waveform inversion algorithm [Fig. 3(b)]. And, we use the observed and calculated stress tensor data; the normal-stress tensors don't have directional component in acoustic case.

The number of shots is 265 and the interval between the shots is 0.020 km. The number of recording channels is 530 and the receiver interval is 0.020 km. The total recording time is 5 s and the time step is 0.002 s. First, we test the feasibility of the source estimation algorithm to investigate the wavelet used. We used the first derivative of a Gaussian function with a 15 Hz cutoff frequency for forward modeling, to produce the estimated source wavelet for each updated velocity model.

Fig. 4 shows a comparison between the signals using the first derivative of a Gaussian function and the estimated wavelet. Fig. 4 shows that the agreement improve as the number of iterations increase. We also perform the proposed waveform inversion algorithm for the modified Marmousi2 model with source wavelet estimation. Fig. 5 shows the inverted P-velocity model at the 50th iteration; the velocity and geologic shape are in agreement with the true velocity model. Fig. 6 shows depth-velocity profiles of the true and inverted velocity models at horizontal position 6.0 km in Fig. 5. Although the inverted velocity model obtained by the proposed algorithm is not an exact match at greater depths, it has a similarity in trend to the depth profile of the true velocity model.

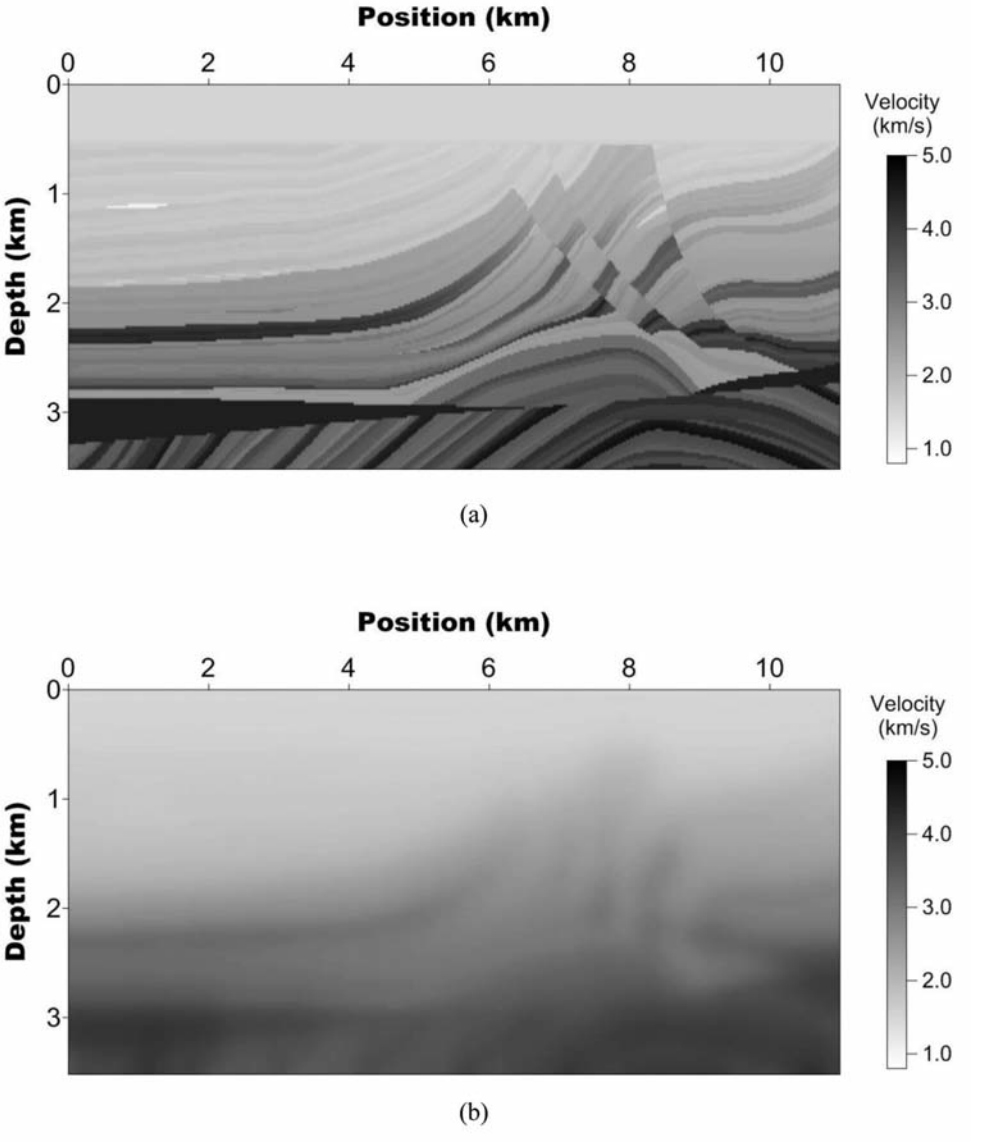

Fig. 3. (a) True and (b) initial P-velocity model.

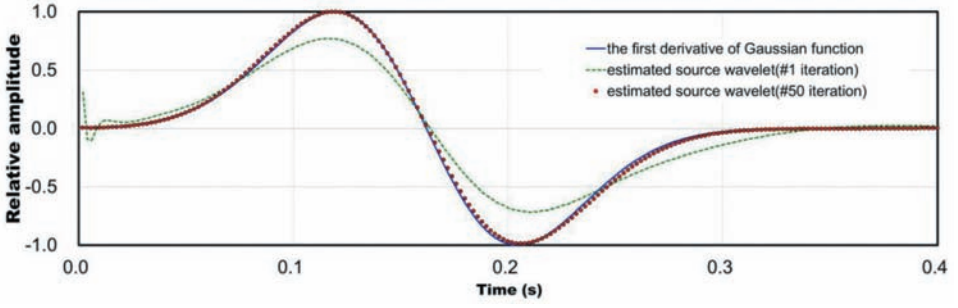

Fig. 4. Comparison of the 1st derivative Gaussian function (solid line), 1st estimated wavelet (dashed line) and 50th estimated wavelet (dotted).

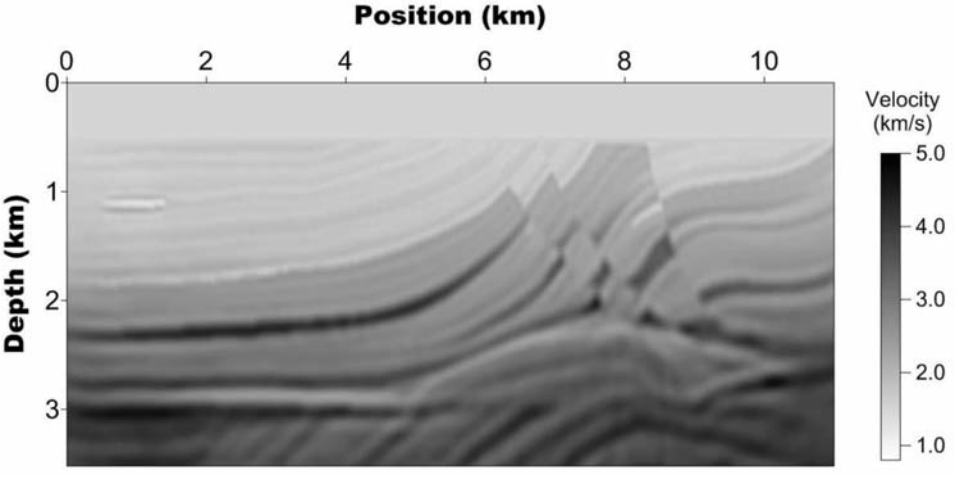

Fig. 5. Inversion result of the Marmousi2 model.

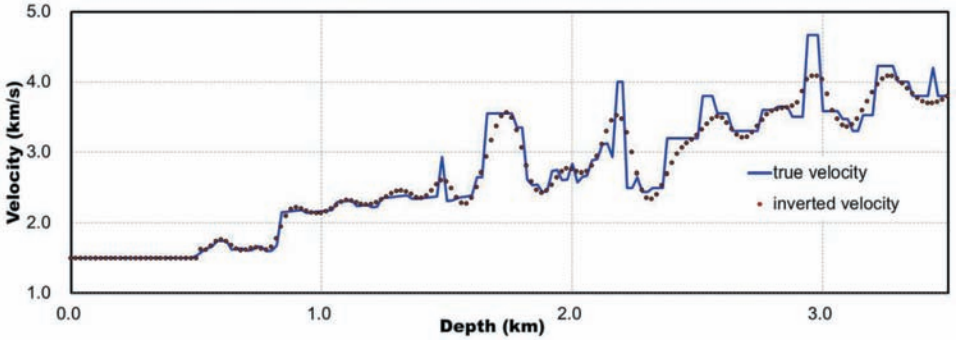

Fig. 6. Depth profiles of the true and inverted velocity by waveform inversion at a horizontal position of 6 km.

To determine the accuracy of both the estimated source and the final updated velocity information, we compare observed and calculated stress seismograms in Fig. 7(a) and (b), respectively; the calculated seismogram is similar to the observed seismogram. To facilitate a specific comparison, we show extracted single observed and calculated traces at 5.5 km from the source in Fig. 8. The predicted trace is very similar to the observed trace.

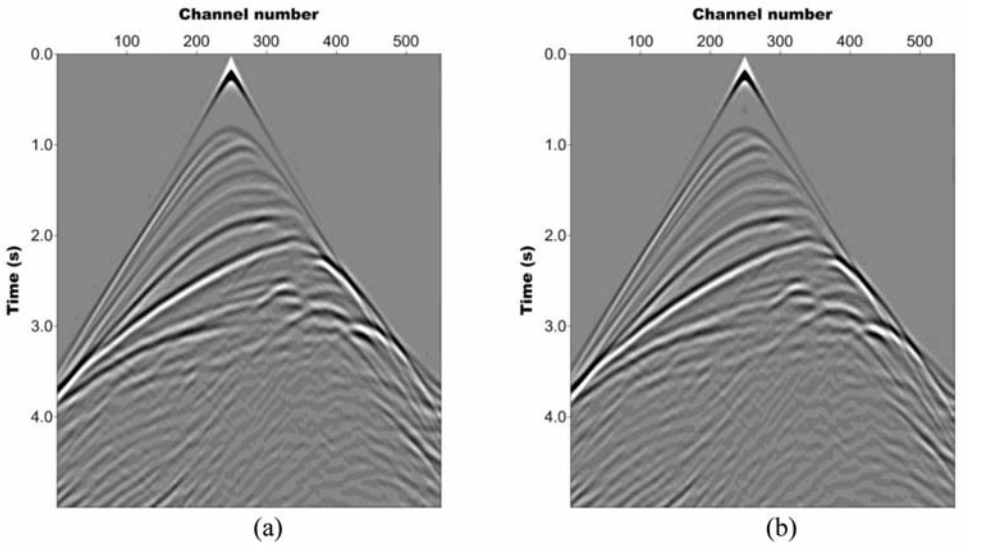

Fig. 7. Comparison of (a) observed data from the true velocity model and (b) calculated data from the inverted velocity model.

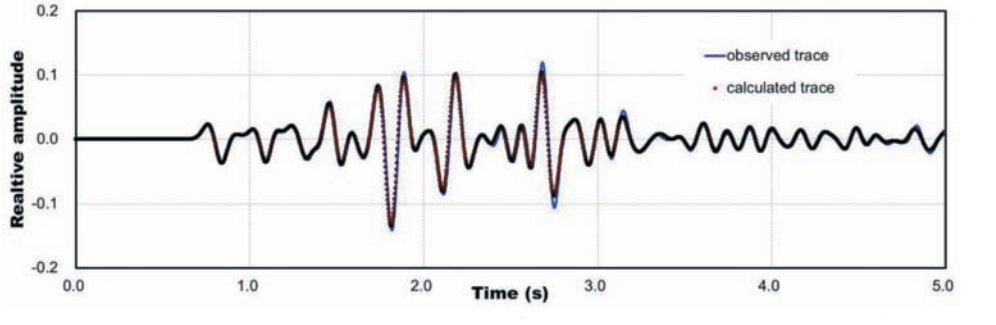

Fig. 8. Comparison of observed and calculated traces at a distance 5.5 km from the source position at the 50th iteration.

The field data set from the East Sea in Korea

The testing of the proposed waveform inversion algorithm is successfully completed in the previous section. However, synthetic data doesn't have the same intrinsic characteristics that real seismic data have, such as various types of random noise associated with the survey environments. Therefore, we apply the proposed waveform inversion algorithm to determine its feasibility using field seismic data.

These data are acquired in the East Sea, Korea, at water depths of approximately 2.0 km. The number of shots is 101, and the shot interval is 0.025 km. The data are obtained using 420 receiver channels; the near offset is 0.125 km and the channel interval is 0.0125 km. The total recording time is 5 s and the time step is 0.001 s.

Fig. 9(a) contains a representative shot gather from the observed data, and Fig. 9(b) shows the initial velocity model. The initial velocity model has linearly increasing from 1.48 km/s at the sea floor to 2.50 km/s at the maximum depth. Fig. 10 shows the wavelet estimated from the field seismic data.

We test the proposed waveform inversion algorithm for the field data set with the estimated source wavelet. Fig. 11 illustrates the inverted velocity model obtained by the proposed waveform inversion algorithm. To evaluate the applicability of the estimated source information and the inverted velocity model, by the proposed algorithm. Fig. 12 illustrates the comparison of two pairs of observed and calculated traces. The direct wave of the calculated data is similar to observed data in Fig. 12(a). In Fig. 12(b), the amplitude of the direct wave has decreased compared to that in Fig. 12(a) because of the increase in geometrical spreading and attenuation with increasing offset. Also, because of the back-ground noise during the survey, there is some interference at the time of the direct wave. In particular, because low frequency information for performing the waveform inversion is poor, the practical source estimation is not easy. The trace of the 1st channel shows a better match than the trace of the 210th channel in the observed data because the signal-to-noise ratio is higher. Although, the complicated reflection events of the calculated data have discrepancies with the observed data, they agree qualitatively in Fig. 12. Fig. 13 shows the decreasing trend of the relative error value with iteration number. The error value reaches a minimum near iteration number 800. The value of the error function is decreased by about 35%. It seems that the survey field is not for an acoustic medium and there may be a loss of low frequency information by frequency filtering for removal of noise. Also, because the velocity range of the initial velocity model may not be accurate, there is a limit to the amount of improvement that is possible in the accuracy of the result of the waveform inversion.

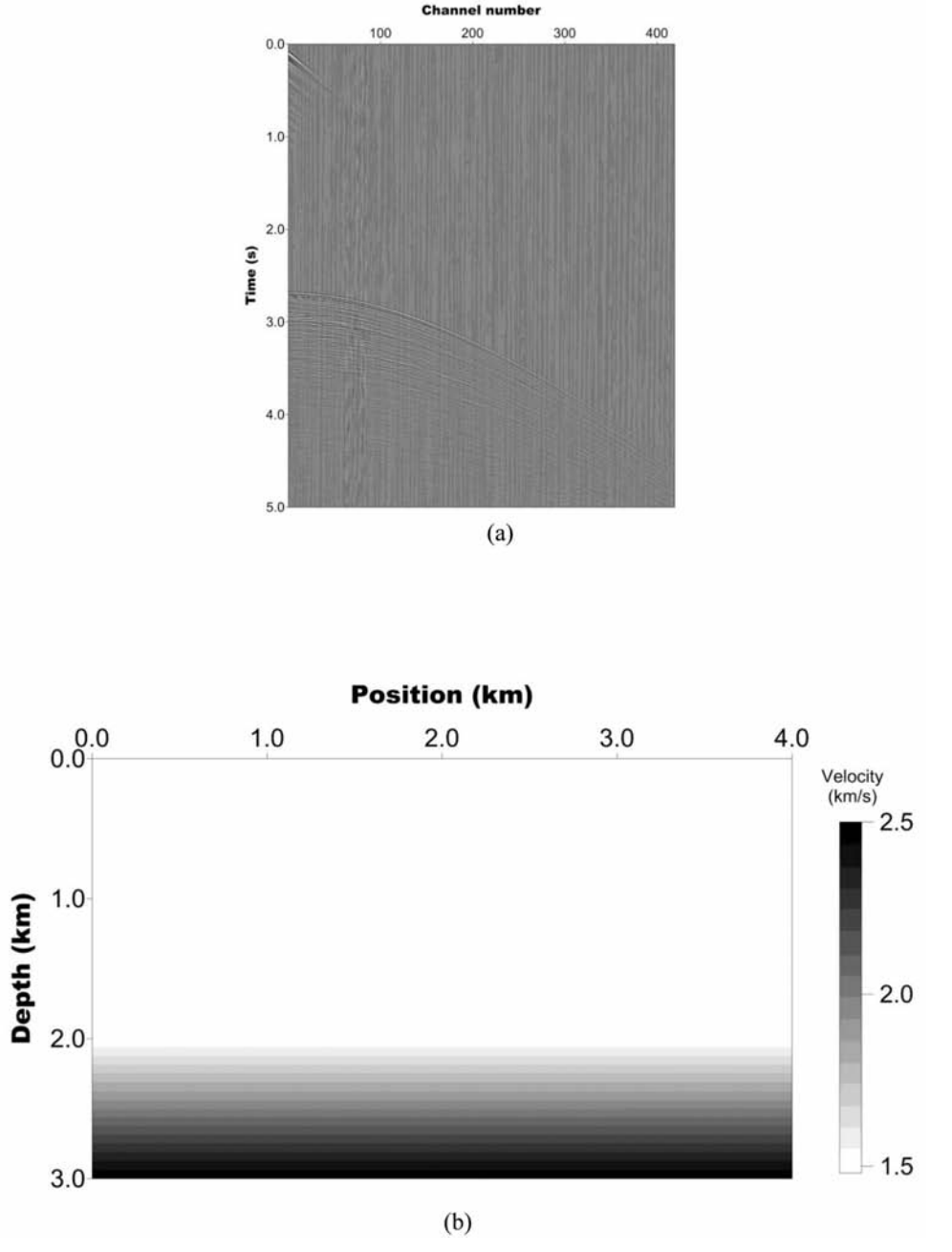

Fig. 9. (a) A raw shot gather and (b) the initial velocity model.

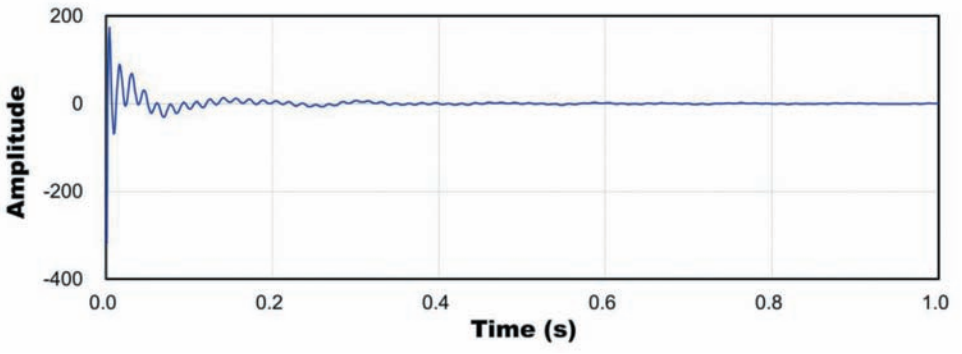

Fig. 10. Estimated source wavelet.

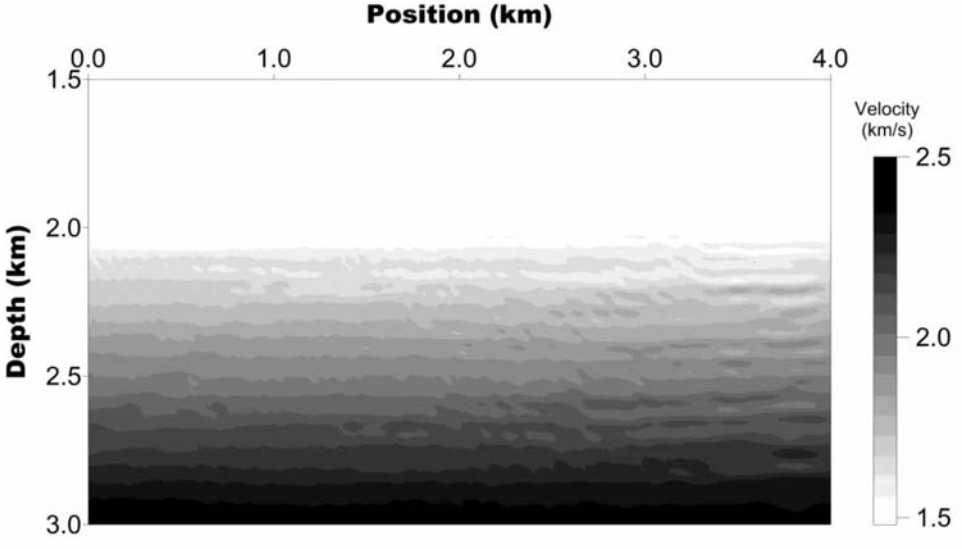

Fig. 11. Inversion result of real data.

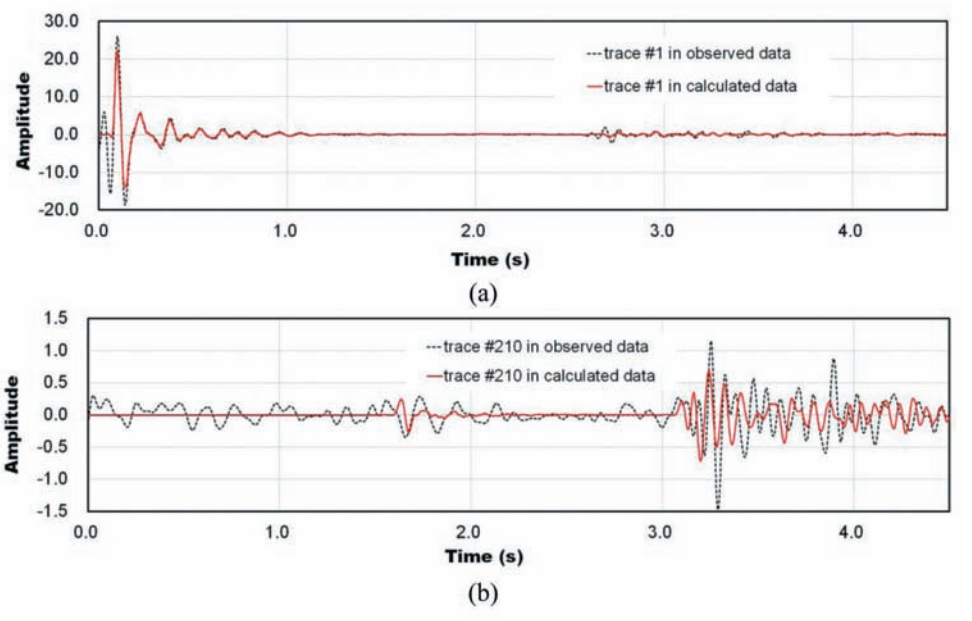

Fig. 12. Comparison of observed and calculated traces from (a) the 1st receiver and (b) the 210th receiver.

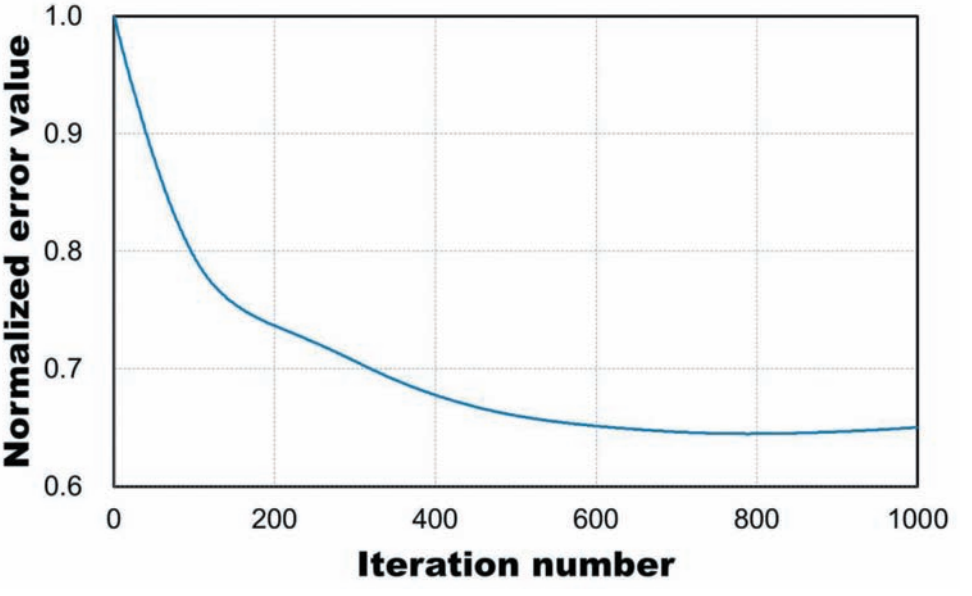

Fig. 13. The relative error as a function of iteration number.

CONCLUSIONS

We apply the pseudo-Hessian method and the back-propagation technique to a full waveform inversion with an estimated source wavelet in the time domain. Defining the virtual source vector is important when using these methods. The virtual source vector is the derivative of the modeling operator with respect to the model parameters. The virtual source depends on the type of modeling algorithm; we derive the virtual source vector based on a 2D staggered-grid modeling technique. The derived virtual source vectors are tested by comparison between two partial derivative wavefields. One is obtained by the virtual sources, and the other is obtained by the finite difference method.

Using both the virtual source vectors and the back-propagated wavefield, the updated gradient direction can be obtained without explicit calculation of the partial derivative wavefield. The pseudo-Hessian method with the gradient direction can enhance the computational efficiency of the proposed waveform inversion. Accurate information on the source wavelet can improve the accuracy of the inversion results when applying the inversion technique to field datasets. We estimate the source wavelet by deconvolution from the observed data based on a least-squares method.

We test the proposed inversion algorithm on synthetic data for a modified Marmousi 2 model. The inverted velocity model is a smoothed version of the true velocity model. Even though the inverted velocity information at the greater depths provides an incomplete match, the depth-velocity profile variation is similar. In addition, the calculated synthetic seismogram with the inverted velocity and the estimated source wavelets shows good agreement with the synthetic observed data. The comparison between the original and the estimated source wavelet shows that the agreement improves as the velocity model is iterating updated.

Finally, we apply the inversion algorithm to field seismic data acquired in the East Sea, Korea. The calculated data using the estimated source wavelet and the inverted velocity model show similar characteristics, including the direct wave. Although we have not obtained an inversion result as good as that for the synthetic data, because of the survey environment, the inverted waveform in the near offset data shows good agreement with the observed waveform. To improve accuracy, a reasonable initial velocity model and estimated source wavelet are needed. Also, data processing considering low frequency components is required. In addition, if interval velocity information from well-logs and a long-wavelength velocity model acquired by other waveform inversion algorithm available, we expect that result of the wavefrom inversion would be improved. These results show that the proposed inversion technique in the time domain can be applied to field seismic data. Also, this waveform inversion algorithm has the advantage that can be easily expanded to migration and to elastic full waveform inversion in the time domain.

ACKNOWLEDGMENTS

This research was supported by the Basic Research Project (15-3314) of the Korea Institute of Geoscience and Mineral Resources (KIGAM) funded by the Ministry of Science, ICT and Future Planning of Korea.

REFERENCES

Bae, H., Shin, C., Cha, Y., Choi, Y. and Min, D.-J., 2010. 2D acoustic-elastic coupled waveform inversion in the Laplace domain. Geophys. Prosp., 58: 997-1010.

Bae, H.-S., Pyun, S., Shin, C., Marfurt, J.K. and Chung, W., 2012. Laplace-domain waveform inversion versus refraction-traveltime tomography. Geophys. J. Internat., 190: 595-606.

Brossier, R., Operto, S. and Virieux, J., 2009. Seismic imaging of complex onshore structures by 2D elastic frequency-domain full-waveform inversion. Geophysics, 74: WCC105-WCC118.

Choi, Y. and Alkhalifah, T., 2011. Source-independent time-domain waveform inversion using convolved wavefield: Application to the encoded multisource waveform inversion. Geophysics, 76: R125- R1234.

Claerbout, J.F., 1971. Toward a unified theory of reflector mapping. Geophysics, 36: 467-481.

Fichtner, A., 2011. Full seismic waveform modeling and inversion. Springer Verlag, Heidelberg, Berlin.

Gauthier, O., Virieux, J. and Tarantola, A., 1986. Two-dimensional nonlinear inversion of seismic waveforms: numerical results. Geophysics, 51: 1387-1403.

Geller, R.J. and Hara, T., 1993. Two efficient algorithms for iterative linearized inversion of seismic waveform data. Geophys. J. Internat.,115: 699-710.

Graves, R.W., 1996. Simulating seismic wave propagation in 3D elastic media, using staggered-grid finite differences. Bull. Seismol. Soc. Am., 86: 1091-1106.

Ha, T., Chung, W. and Shin, C., 2009. Waveform inversion using a back-propagation algorithm and a Huber function norm. Geophysics, 74: R15-R24.

Ha, T., Pyun, S. and Shin, C., 2006. Efficient electric resistivity inversion using adjoint state of mixed finite-element method for Poisson's equation. J. Computat. Phys., 214: 171-186.

Hampson, D.P., Russell, B.H. and Bankhead, B., 2005. Simultaneous inversion of pre-stack seismic data. Expanded Abstr., 75th Ann. Internat. SEG Mtg., Houston: 1633-1637.

Jin, S. and Madariaga, R., 1993. Background velocity inversion by a genetic algorithm. Geophys. Res. Lett., 20: 93-96.

Jin, S. and Madariaga, R., 1994. Non-linear velocity inversion by a two-step Monte Carlo method. Geophysics, 59: 577-590.

Kim, Y., Min, D.-J. and Shin, C., 2011. Frequency-domain reverse time migration with source estimation. Geophysics, 76: S41-S49.

Koo, N.-H., Shin, C., Min, D.-J., Park, K.-P. and Lee H.-Y., 2011. Source estimation and direct wave reconstruction in Laplace-domain waveform inversion for deep-sea seismic data. Geophys. J. Internat., 187: 861-870.

Koren, Z., Mosegaard, K., Landa, E., Thore, P. and Tarantola, A., 1991. Monte Carlo estimation and resolution analysis of seismic background velocities. J. Geophys. Res., 96: 20289-20299.

Lailly, P., 1983. The seismic inverse problem as a sequence of before stack migrations: Conference on Inverse Scattering: Theory and Application. Expanded Abstr., Soc. Industr. Appl. Mathemat. Conf.: 206-220.

Levander, A.R., 1988. Fourth-order finite-difference P-SV seismograms. Geophysics, 53: 1425-1436.

Métivier, L., Bretaudeau, F., Brossier, R., Operto, S., and Virieux, J., 2014. Full waveform inversion and the truncated newton-method: quantitative imaging of complex subsurface structures. Geophys. Prosp., 62: 1353-1375.

Mosegaard, K. and Tarantola, A., 1995. Monte Carlo sampling of solutions to inverse problems. J. Geophys. Res., 100: 12431-12447.

Pratt, P., 1999. Seismic waveform inversion in the frequency domain, part I: Theory and verification in a physical scale model. Geophysics, 64: 888-901.

Pratt, R.G. and Shipp, R.M., 1999. Seismic waveform inversion in the frequency domain, Part 2: Fault delineation in sediments using cross hole data. Geophysics, 64: 902-914.

Pratt, R.G., Shin, C. and Hicks, G.J., 1998. Gauss-Newton and full Newton methods in frequency-space seismic waveform inversion. Geophys. J. Internat., 133: 341-362.

Sambridge, M. and Mosegaard, K., 2002. Monte Carlo methods in geophysical inverse problems. Rev. Geophys., 40: 1-29.

Sheen, D.-H., Tuncay, K., Baag, C.-E. and Peter, J.O., 2006. Time domain Gauss-Newton seismic waveform inversion in elastic media. Geophys. J. Internat., 167: 1373-1384.

Shin, C. and Cha, Y., 2008. Waveform inversion in the Laplace domain. Geophys. J. Internat., 173: 922-931.

Shin, C. and Min, D., 2006. Waveform inversion using a logarithm wavefield. Geophysics, 71: R31-R42.

Shin, C., Jang, S. and Min, D.-J., 2001. Improved amplitude preservation for prestack depth migration by inverse scattering theory. Geophys. Prosp., 49: 592-606.

Shin, C., Pyun, S. and Bednar, J.B., 2007. Comparison of waveform inversion, part 1: conventional wavefield vs. logarithmic wavefield. Geophys. Prosp., 55: 449-464.

Shin, C., Yoon, K., Marfurt, K.J., Park, K., Yang, D., Lim, H.Y., Chung, S. and Shin, S., 2001. Efficient calculation of a partial-derivative wavefield using reciprocity for seismic imaging and inversion. Geophysics, 66: 1856-1863.

Tarantola, A., 1984. Inversion of seismic reflection data in the acoustic approximation. Geophysics, 49: 1259-1266.

Toxopeus, G., Thorbecke, J., Wapenaar, C.P.A., Petersen, S., Slob, E. and Fokkema, J.T., 2008. Simulating migrated and inverted seismic data by filtering a geologic model. Geophysics, 73: T1-T10.

Virieux, J., 1986. P-SV wave propagation in heterogeneous media: velocity-stress finite-difference method. Geophysics, 51: 889-901.

Virieux, J. and Operto, S., 2009. An overview of full-waveform inversion in exploration geophysics. Geophysics, 74: WCC1-WCC26.

Zong, Z., Yin., X. and Wu, G., 2013. Multi-parameter nonlinear inversion with exact reflection coefficient equation. J. Appl. Geophys., 98: 21-32.